

Raman Scattered Ne VII λ 973 at 4881 Å in the Symbiotic Star V1016 Cygni

Hee-Won Lee,^{1*} Jeong-Eun Heo,^{1†} and Byeong-Cheol Lee^{2‡}

¹*Department of Astronomy and Space Science, Sejong University, Seoul, 143-747, Korea*

²*Korea Astronomy and Space Science Institute, Daejeon, Korea*

Accepted 1988 December 15. Received 1988 December 14; in original form 1988 October 11

ABSTRACT

We present the high resolution spectra of the symbiotic star V1016 Cygni obtained with the Bohyunsan Optical Echelle Spectrograph in 2003 and 2005, from which we find a broad emission feature at 4881 Å. We propose that this broad feature is formed from Raman scattering of Ne VII λ 973 by atomic hydrogen. Thus far, the detection of Raman scattered lines by atomic hydrogen is limited to O VI λ 1032, 1038 and He II λ 940, 972 and 1025. With the adoption of the center wavelength 973.302 Å of Ne VII λ 973 and consideration of the air refractive index of $n_{air} = 1.000279348$, the atomic line center of the Raman scattered Ne VII feature is determined to be 4880.53 Å. The total cross section at the line center of Ne VII λ 973 is computed to be 2.62×10^{-22} cm² with the branching ratio of 0.17. We perform Monte Carlo simulations to fit the Raman scattered Ne VII λ 973. Assuming that the Ne VII and He II emission regions share the same kinematics with respect to the neutral scattering region, we find that the Raman scattered He II λ 972 at 4850 Å and Ne VII λ 973 at 4881 Å are excellently fitted. We also propose that the He II and Ne VII emission regions were stationary with respect to the H I region in 2003 but that they were receding from it with a velocity ~ 20 km s⁻¹ in 2005.

Key words: binaries: symbiotic – atomic processes – line: identification – scattering – stars (individual V1016 Cyg)

1 INTRODUCTION

Symbiotic stars are believed to be wide binary systems consisting of a hot component, usually a white dwarf, and a mass losing giant (e.g. Kenyon 1986, Belczynski et al. 2004). Because of the size of the giant component, their orbital periods range from a few hundred days to several decades (e.g. Mikolajewska 2012). Symbiotic stars exhibit prominent emission lines indicative of a wide range of ionization including [SII] and O VI. Some fraction of the slow stellar wind from the giant component is accreted to the hot component, which leads to various activities including occasional eruptions and strong emission lines (e.g. Iben & Tutukov 2004, Lee & Park 1999). Mastrodemos & Morris (1998) performed *Smoothed Particle Hydrodynamical* computations for binary systems of a mass losing giant and a white dwarf to show that an accretion disk may be formed through accretion of the stellar wind. However, it is still an unresolved

issue whether an accretion disk is formed in general in symbiotic stars (e.g. Sokoloski et al. 2001, Nussbaumer 2003).

Symbiotic stars are classified into 'S' type and 'D' type, where the latter exhibit an IR excess indicating the existence of a warm dust component surrounding the binary system. It appears that D-type symbiotic stars possess multiple dust shells with temperatures of $\simeq 1000$ K and $\simeq 400$ K (Angeloni et al. 2010). Many symbiotic stars are also X-ray emitters exhibiting a large range of hardness. Luna et al. (2013) classified X-ray emitting symbiotic stars into types α , β , γ and δ depending on the hardness with the α type being supersoft X-ray sources and the δ type being highly absorbed hard X-ray emitters. They discussed many astrophysical processes including thermonuclear shell burning, wind collision and boundary layer in the accretion disk.

In symbiotic stars unique and useful spectroscopic diagnostics are provided from Raman scattering by atomic hydrogen. In this scattering process, a far UV photon blueward of Ly α is incident upon a hydrogen atom in the ground state. Subsequently the hydrogen atom de-excites into 2s state re-emitting an optical Raman-scattered photon. The first identification of Raman scattering in symbiotic stars was made by Schmid (1989), who proposed that the broad

* E-mail: hwlee@sejong.ac.kr (HWL)

† E-mail: jeung6145@gmail.com

‡ E-mail: bclee@kasi.re.kr

emission features at 6825 Å and 7088 Å usually observed in many symbiotic stars are Raman scattered O VI λ 1032 and O VI λ 1038. The operation of Raman scattering requires the coexistence of a highly thick H I region and a strong far UV emission region, which is ideally met in symbiotic stars. Recently Raman scattered O VI 1032 and 1038 features were found in the B[e] star LHA 115-S 18 (Torres et al. 2012).

Raman spectroscopy is very important in probing the mass loss and mass transfer processes in symbiotic stars (e.g. Schmid 1989, Lee & Park 1999). Adopting an emission region that is in a Keplerian motion around the hot component, Lee & Kang (2007) successfully fitted the double peaked profiles of the Raman scattered O VI λ 1032 of the symbiotic stars HM Sge and V1016 Cygni. The representative Keplerian velocity scale $\sim 30 \text{ km s}^{-1}$ of the emission regions in these two symbiotic stars implies that the major O VI emission region is located roughly within one astronomical unit from the hot component. It should be also noted that a double peak profile in Raman scattered O VI can be produced from purely geometric effects, where the scattering region coincides with the slowly expanding stellar wind around the giant (e.g. Harries & Howarth 1997, Schmid 1992). The mass loss rate of the cool component of V1016 Cyg has been deduced from a photoionization model calculation combined with the measurement of the center shift of Raman scattered He II by Jung & Lee (2004).

Additional Raman scattered features were found and proposed by van Groningen (1993), who discussed the plausibility of Raman scattering for various far UV emission lines including He II and C III. In particular, he reported the detection of the Raman scattered He II features blueward of H β and H γ in the symbiotic star RR Telescopii. These features are also found in the symbiotic stars HM Sge and V1016 Cyg (e.g. Birriel 2004, Jung & Lee 2004, Lee 2012).

In a Be-like isoelectronic sequence, Ne VII is a very highly ionized species with the ionization potential of 207.271 eV (e.g. Kramida et al. 2013). Because of this high ionization potential, Ne VII lines are reported only in extremely hot stellar objects and active galactic nuclei. Werner et al. (2004) found Ne VII λ 973 absorption lines in the spectra of PG 1159 stars obtained with the *Far Ultraviolet Spectroscopic Explorer (FUSE)*. Young et al. (2005) proposed the existence of Ne VII λ 973 in the FUSE spectrum of the symbiotic star AG Draconis. In the Seyfert 1 galaxy NGC 5548 Kaastra et al. (1995) identified Ne VII/Ne VIII blend at 88 Å in the extreme UV spectrum.

V1016 Cyg is a 'D' type symbiotic star with the cool component being a Mira type variable. It is also a symbiotic nova that underwent a nova-like outburst in 1964 (McCusky 1965). According to the investigation of Mürset et al. (1991), 'D' type symbiotic novae including HM Sge, RR Tel and V1016 Cyg form the subgroup of symbiotic stars with the hot components characterized by the highest temperature and luminosity. V1016 Cyg being of higher temperature than AG Dra, this leads to an interesting possibility that V1016 Cyg may show the emission line Ne VII λ 973.

In this paper, we present the high resolution spectra of V1016 Cyg, in which a broad emission feature at 4881 Å is found redward of H β . We propose this broad feature is formed through Raman scattering of the far UV emission line Ne VII λ 973 in the thick H I region.

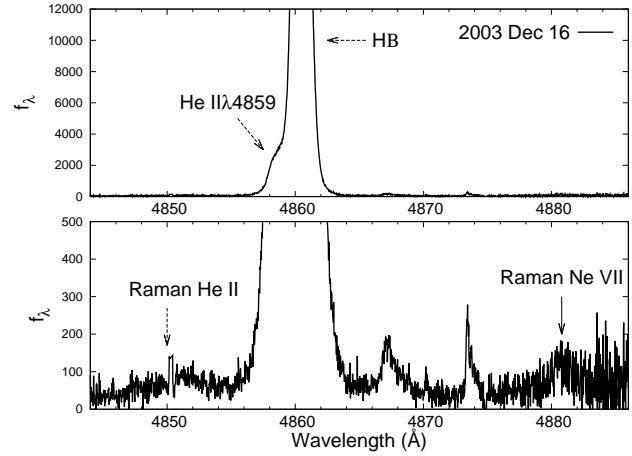


Figure 1. The high resolution spectrum of V1016 Cyg near H β obtained with BOES on 2003 December 16. The lower panel is a blow-up version of the upper panel by a factor 24. The vertical axis shows the CCD counts. The broad feature around 4882 Å marked by the solid vertical arrow shown in the bottom panel is proposed to be Raman scattered Ne VII λ 973 by atomic hydrogen.

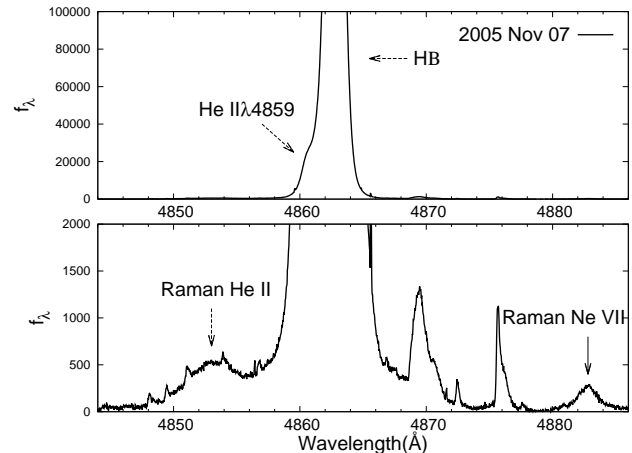


Figure 2. The high resolution spectrum of V1016 Cyg obtained with BOES on 2005 November 7. The lower panel is a blow-up version of the upper panel by a factor 50. The vertical axis shows the CCD counts. The same broad feature is found around 4883 Å which is marked by the solid vertical arrow shown in the bottom panel.

2 OBSERVATION

2.1 High resolution spectroscopy of V1016 Cyg

Fig. 1 shows a high resolution spectrum of V1016 Cyg obtained with the Bohyunsan Optical Echelle Spectrograph (BOES) installed on the 1.8 m optical telescope at Mt. Bohyun on the night of 2003 December 16. In Fig. 2, we show another BOES spectrum of V1016 Cyg obtained on 2005 November 7. For the spectrum of 2003, the 200 μm optical fiber was used to yield the spectroscopic resolution of $\simeq 44,000$. On the other hand, the 2005 spectrum was obtained using the 300 μm optical fiber achieving spectroscopic

resolution of $\simeq 30,000$. The exposure time was 3000 seconds and 7200 seconds for the spectrum of 2003 and that of 2005, respectively. In Fig. 1, the lower panel is a blow-up version of the upper panel by a factor 24. In a similar way, in Fig. 2 the scale of the lower panel is 50 times smaller than that of the upper panel.

In the 2005 spectrum, the emission line $H\beta$ is saturated in order to allow a close investigation of the weak features around $H\beta$. We also obtained another spectrum with a short exposure time of 300 seconds, which is shown in Fig. 3. As in the analysis of Jung & Lee (2004) we find Raman scattered He II λ 972 at 4850 Å in the two long exposure spectra obtained in 2003 and 2005, which is very broad and formed in the blue wing part of $H\beta$.

Because of energy conservation, the wavelength λ_{RV} of the Raman scattered radiation in vacuum is related to that of the far UV incident radiation λ_i by the equation

$$\lambda_{RV} = \frac{\lambda_{Ly\alpha}\lambda_i}{\lambda_{Ly\alpha} - \lambda_i}, \quad (1)$$

where $\lambda_{Ly\alpha} = 1215.67$ Å is the line center wavelength of hydrogen Ly α . With the refractive index of air $n_{air} = 1.000279348$, the observed wavelength will be reduced to

$$\lambda_R = \lambda_{RV}/n_{air}. \quad (2)$$

In particular, the incident wavelength $\lambda_i = 972.112$ Å for He II λ 972 gives rise to the Raman scattered He II at $\lambda_{RV,HeII} = 4852.098$ Å (Jung & Lee 2004), which yields the observed wavelength of $\lambda_{R,HeII} = 4850.743$ Å.

In Fig 1, the broad Raman scattered He II feature has the observed line center at $\lambda_{R,HeII}^{obs} = 4850.63$ Å, which is blueshifted from $\lambda_{R,HeII}$ by $\Delta\lambda = 0.11$ Å from the expected center wavelength. On the other hand, in Fig. 2, we find that $\lambda_{R,HeII}^{obs} = 4852.95$ Å. This deviation can be explained that the He II emission region is receding from the neutral H I region. More detailed investigation on the kinematics of the emission region is described in the subsequent section. However, line center shift can also occur due to the varying Raman conversion rate dependent on the wavelength (Jung & Lee 2004), which necessitates Monte Carlo simulations for more accurate determination of the kinematics of the He II emission region relative to the H I region.

Eq. (1) also leads to the following relation

$$\frac{\Delta\lambda_R}{\lambda_R} = \left(\frac{\lambda_R}{\lambda_i}\right) \frac{\Delta\lambda_i}{\lambda_i}, \quad (3)$$

which results in Raman scattered features with a significantly broadened profile. In particular, the Raman scattered features around $H\beta$ are broadened by a factor $\lambda_R/\lambda_i \simeq 5$, because $\lambda_i \simeq 972$ Å and $\lambda_R \simeq 4861$ Å.

Using a Gaussian function given by

$$F(\lambda) = F_0 \exp[-(\lambda - \lambda_0)^2/\Delta\lambda^2], \quad (4)$$

we perform a line profile fitting analysis to determine the observed centers of the emission lines He II λ 4859 and $H\beta$ in the 2005 spectrum of V1016 Cyg. Because of the saturation of $H\beta$, we use another spectrum obtained on the same night with an exposure time of 300 seconds. In Fig. 3, we show the result, which is also summarized in Table 1.

In a similar way, the Raman scattered He II λ 972 and the broad feature at 4883 Å are fitted for the spectrum with exposure time of 7200 seconds, of which the result is shown

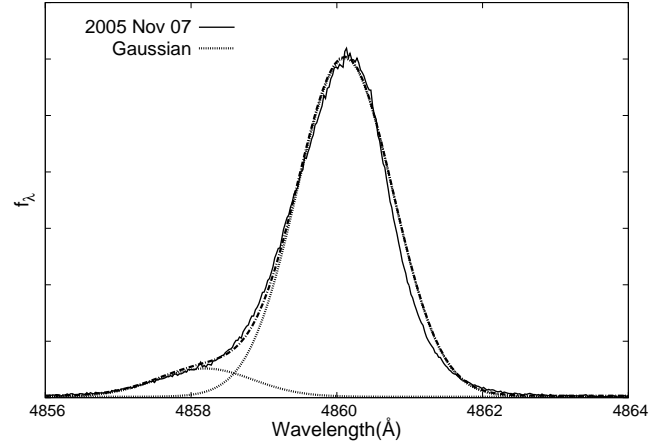


Figure 3. Profile fit of He II λ 4859 and $H\beta$ using a single Gaussian function for the spectrum obtained on the night of 2005 November 7 with the exposure time of 300 seconds. Gaussian fitting functions are shown by dotted lines and the BOES spectrum is represented by a solid line. The BOES data are fitted by combining the two Gaussian functions, which is represented by a dot-dashed line. The observed line center of He II λ 4859 is 4858.57 Å and that of $H\beta$ is 4860.54 Å.

in Fig. 4. For this, the broad $H\beta$ wings are fitted using a profile $(\lambda - \lambda_\beta)^{-2}$, where λ_β is the wavelength of $H\beta$. In the case of the 2003 spectrum, the profile fitting was done by Jung & Lee (2004) except the broad feature at 4881 Å. In this work, the observed line center of this feature in the 2003 spectrum is determined to be 4880.80 Å. The result of our single Gaussian fit to the 2003 spectrum is also summarized in Table 1.

2.2 Raman scattered Ne VII λ 973

Both in Figs. 1 and 2, the broad emission feature marked by a solid vertical arrow is noticeable. This feature in the 2003 spectrum is very weak with the observed center at 4880.80 Å but it is significantly clear at 4882.82 Å in the spectrum of 2005 with much longer exposure time. We propose that this broad feature is formed through Raman scattering of Ne VII λ 973 by atomic hydrogen.

Ne VII λ 973 is formed through recombination of Ne VIII accompanied by a radiative transition from $2p^2\ ^1D_2$ to $2s2p\ ^1P_1$ (e.g. Young et al. 2005). This line was also found in the high resolution coronal spectrum of the sun obtained with the Solar Ultraviolet Measurement of Emitted Radiation (SUMER) on board the *Solar and Heliospheric Observatory*, *SOHO* (Feldman et al. 1997). Herald et al. (2005) proposed that Ne VII λ 973 is responsible for the strong P Cygni features observed at around 975 Å for a number of hot evolved stars including A78, NGC 2371 and K1-16.

The atomic data for Be-isoelectronic atoms can be found in the work of Edlén (1983), who compared the theoretical values with the experimental data. He recommended the values of 214954 cm^{-1} and 317954 cm^{-1} for the lower and the higher energy levels respectively, from which the center wavelength of Ne VII λ 973 is obtained to be 973.350 Å. However, according to Kramida et al. (2013), the en-

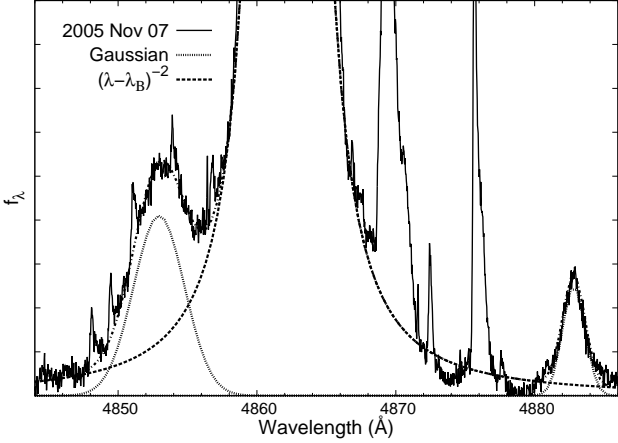


Figure 4. Profile fit of Raman scattered He II $\lambda 972$ and a broad feature at 4883 \AA using a single Gaussian function for the spectrum obtained on the night of 2005 November 7 with the exposure time of 7200 seconds. For the $H\beta$ wing the profile function proportional to $(\lambda - \lambda_\beta)^{-2}$ is used for fitting, which is shown by a thick dotted line. The BOES spectrum is shown by a solid line and the two single Gaussian functions are represented by a dotted line. The dot-dashed line shows the combined fit of the two Gaussians and $H\beta$ wing. The observed line center of Raman scattered He II $\lambda 972$ is 4852.95 \AA and that of Raman scattered Ne VII $\lambda 973$ is 4882.82 \AA .

ergy values of the lower and the higher levels are 214951.6 cm^{-1} and 317694.6 cm^{-1} respectively, resulting in the central wavelength of 973.302 \AA . This result is based on the previous work of Kramida et al. (2006). In this work we adopt this value as the line center wavelength $\lambda_0 = 973.302 \text{ \AA}$ of Ne VII $\lambda 973$.

A direct substitution of the Ne VII line center wavelength into Eq. (1) yields the vacuum line center wavelength of the Raman scattered Ne VII feature, which is given by $\lambda_{Ne}^{RV} = 4881.89 \text{ \AA}$. Considering the refractive index of air, this vacuum wavelength is reduced to

$$\lambda_{Ne}^R = 4880.53 \text{ \AA}, \quad (5)$$

from which we propose to call this broad feature 'Raman scattered Ne VII $\lambda 973$ '. In Section 3, we perform Monte Carlo simulations to fit the profile, from which we may deduce useful constraints on the strength and profile of the unobserved Ne VII $\lambda 973$.

This line center value λ_{Ne}^R is shorter than the observed center wavelength $\lambda_R^{obs} = 4880.80 \text{ \AA}$ by a small amount of $\Delta\lambda = 0.27 \text{ \AA}$ in the 2003 spectrum. In the case of the 2005 spectrum, the corresponding values are $\lambda_R^{obs} = 4882.82 \text{ \AA}$, and $\Delta\lambda = 2.29 \text{ \AA}$. This feature is quite broad, which is consistent with the primary characteristic of a Raman scattered feature. A similar spectroscopic behavior is seen in the case of Raman scattered He II $\lambda 972$. In the 2003 data, the observed line center of Raman scattered He II $\lambda 972$ is almost coincident with that expected from the atomic line center. However, in the 2005 spectrum it is redshifted by an amount exceeding 2 \AA . Because both He II and Ne VII are highly ionized species, it is quite plausible that their emission regions almost coincide sharing a similar kinematics with respect to

the neutral region. Because the profiles of Raman scattered features are dominantly affected by a relative motion between the far UV emission source and the H I region and little influenced by the observer's sightline, the difference in the spectra of 2003 and 2005 implies that there was a significant change in the far UV emission region and/or in the H I region of V1016 Cyg.

2.3 Temporal Variation of the Kinematics of the Far UV Emission Regions

We investigate the temporal change in relative velocities of the He II emission region and Ne VII emission region with respect to the neutral H I region, which may have happened during the two year period. In this work, the atomic line center of $H\beta$ is set to be $\lambda_\beta = 4861.28 \text{ \AA}$ in air and we assume that the Balmer emission region suffered no significant changes in kinematics. In Table 2, we provide the observed wavelengths corrected for the rest frame of $H\beta$ emission region. It is unclear whether the Balmer emission region may represent the systemic velocity of V1016 Cyg due to some variability in this wide binary system. However, a reference system is useful in discussion of the relative motion of the He II and Ne VII emission regions and we take the Balmer emission region as a kinematic reference.

In Table 2, we also show the line center wavelengths of Raman scattered He II $\lambda 972$, He II $\lambda 4859$ and Raman scattered Ne VII $\lambda 973$ corrected for the rest frame of $H\beta$. In the year 2003, the corrected line center of He II $\lambda 4859$ almost coincides with that of the atomic line center, implying that at that time the He II emission region is almost stationary with respect to the Balmer emission region. Despite this, Raman scattered He II $\lambda 972$ is redshifted by an amount 0.63 \AA . This redward shift is attributed to the atomic physical effect, which was pointed out by Jung & Lee (2004). According to them, the scattering cross section and branching ratio are increasing functions of wavelength locally around the line center of He II $\lambda 972$. This enhances Raman scattered radiation redward of He II $\lambda 972$, resulting in an overall redward shift of the Raman scattered feature. The exact amount of wavelength shift depends on the H I column density N_{HI} . Their Monte Carlo simulations yielded the value of $N_{HI} = 1.2 \times 10^{21} \text{ cm}^{-2}$ for V1016 Cyg.

However, the wavelength shift of 3.38 \AA of Raman scattered He II $\lambda 972$ shown in the 2005 spectrum is too large to be accounted for by the effect of atomic physics. This implies that the He II emission region was receding from the H I region at the time of the observation in 2005. Both the Doppler shift and the atomic physics affect the wavelength shift in a complicated way so that one requires Monte Carlo simulations in order to determine the kinematics of the He II and Ne VII emission regions. Exactly the same argument applies to the Raman scattered Ne VII $\lambda 973$, which constitutes the content of the following section.

3 MONTE CARLO SIMULATIONS

3.1 Cross sections and branching ratios

The scattering cross section is computed from the second order time-dependent perturbation theory described

Table 1. Observed wavelengths of emission lines and Raman scattered features in the two high resolution spectra of V1016 Cyg

Line Observed Wavelength	Raman He II λ 972 at 4850 λ_{4850}^{obs}	He II λ 4859 λ_{4859}^{obs}	H β λ_{β}^{obs}	Raman Ne VII λ 973 at 4881 λ_{4881}^{obs}
2003 Dec 16	4850.63	4858.57	4860.54	4880.80
2005 Nov 07	4852.95	4858.19	4860.11	4882.82
Atomic Line Center	4850.74	4859.32	4861.28	4880.53

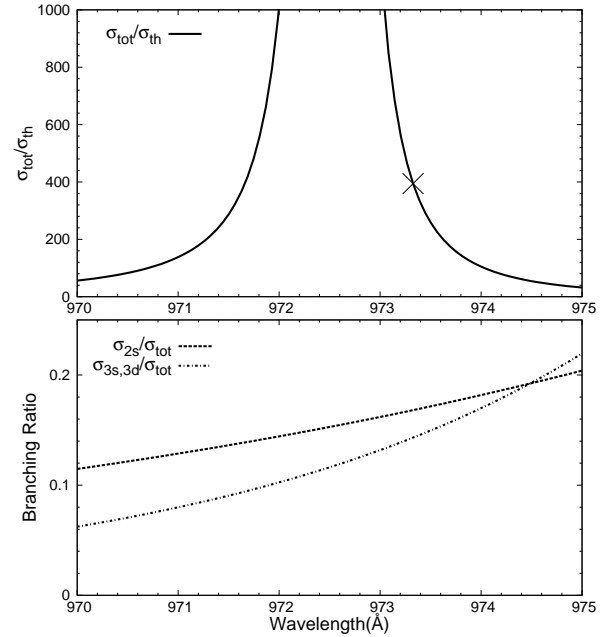
Table 2. Difference of the observed line wavelength from that of the observed H β

Line Wavelength Corrected	Raman He II λ 972at4850 λ_{4850}	He II λ 4859 λ_{4859}	Raman Ne VII λ 973 at 4881 λ_{4881}
2003 Dec 16	4851.37	4859.31	4881.54
2005 Nov 07	4854.12	4859.36	4883.99

in many textbooks on quantum mechanics including Bethe & Salpeter (1957). The cross section is given by the Kramers-Heisenberg formula, where the matrix elements are provided in a straightforward way in the case of a single electron atom such as hydrogen. Blueward of Ly γ , there are 4 scattering channels depending on the principal quantum number of the final state of the hydrogen atom, where the final state can be the s states of $n = 1$ and $n = 2$, and the s and d states of $n = 3$ and 4. Redward of Ly γ , states with $n = 4$ are excluded from the final state, leaving only 3 scattering channels. When the final state is $2s$, then we have optical scattered radiation near H β . Final states with $n = 3$ and $n = 4$ lead to Raman scattered radiation in the IR region. The total scattering cross section σ_{tot} and the branching ratios around Ly γ were computed and presented by Lee et al. (2006) in their analysis of the Raman scattered He II λ 972 in the young planetary nebula IC 5117.

In Fig. 5 we show the scattering cross section and branching ratios near Ly γ computed by Jung & Lee (2004). The upper panel shows the total scattering cross section in units of the Thomson scattering cross section $\sigma_{Th} = 0.665 \times 10^{-24} \text{ cm}^2$. For $\lambda = 973.302 \text{ \AA}$ the total scattering cross section $\sigma_{tot} = 394\sigma_{Th} = 2.62 \times 10^{-22} \text{ cm}^2$, which is marked by a cross in the figure. In the lower panel, the dotted line shows the branching ratio σ_{2s}/σ_{tot} for Raman scattering into the optical channel, where σ_{2s} is the cross section for the final state of $2s$. Another branching ratio into $n = 3$ levels is shown by a dot-dashed line, which shows the ratio of $\sigma_{3s,3d}/\sigma_{tot}$ with $\sigma_{3s,3d}$ being the cross section for final states of $3s$ and $3d$. We find the branching ratio of 0.168 for the scattering channel into the level $2s$ leading to formation of Raman scattered Ne VII λ 973.

For comparison, we note that the total scattering cross section for He II λ 972 is $9.1 \times 10^{-22} \text{ cm}^2$, which is larger than that of Ne VII λ 973 by a factor of 3.5. This is due to the fact that He II λ 972 is closer to resonant Ly γ than Ne VII λ 973 is. It is interesting to note that the total scattering cross section is decreasing but the branching ratio is slowly increasing as a function of wavelength locally around Ne VII λ 973.


Figure 5. Atomic data for Rayleigh and Raman scattering around Ly γ . In the upper panel, the total cross section σ_{tot} of Rayleigh and Raman scattering near Ly γ is shown by a solid line. The cross section for Ne VII λ 973.3 is marked with a cross symbol. In the lower panel, the branching ratio of Raman scattering into the $2s$ state is shown by a dotted line and the branching ratio into levels with $n = 3$ is shown by a dot-dashed line.

3.2 Monte Carlo Simulations

Broad Balmer wings are fairly common in symbiotic stars and V1016 Cyg is no exception. Lee (2000) proposed that these wings are formed through Raman scattering of far UV continuum around Lyman series emission lines. It has been also proposed that the hot tenuous fast stellar wind from the hot component is responsible for the Balmer wings in these objects (e.g. Skopal 2006). It is a difficult task to determine unequivocally the origin of the Balmer wings for an individual source. However, in the case of V1016 Cyg, Lee (2012) proposed that the Raman scattering origin of the Balmer

wings is quite plausible in his analysis of Raman scattered He II λ 4332.

In this work we assume that the broad H β wings are also formed through Raman scattering of far UV continuum around Ly γ . To the far UV continuum we add the two emission components of He II and Ne VII so that the input spectrum consists of the following three components, i.e., a locally flat continuum, and the two emission components of He II λ 972 and Ne VII λ 973. Both the emission components are prepared to exhibit a Gaussian profile given by Eq. (4). For the 2003 spectrum, both the He II emission region and the Ne VII λ 973 region are assumed to be at rest with respect to the H I region.

As is shown in the works of Lee (2000) and Jung & Lee (2004), the Raman scattered radiation of far UV continuum around Ly β is characterized by a plateau near the Balmer core and an extended wing approximately proportional to $\Delta\lambda^{-2}$. The extent of the plateau is determined by the scattering optical depth of a few, because the Raman conversion efficiency becomes saturated above this scattering optical depth. Therefore the width of the plateau increases as N_{HI} increases, which may be used to put a constraint on the value of N_{HI} .

Jung & Lee (2004) proposed the neutral hydrogen column density $N_{HI} = 1.21 \times 10^{21} \text{ cm}^{-2}$ in their analysis of Raman scattered He II λ 972 in V1016 Cyg. With a column density exceeding $N_{HI} = 5 \times 10^{21} \text{ cm}^{-2}$, Raman scattered He II λ 972 is formed in the plateau part of the H β wing, which is inconsistent with our BOES data. On the other hand, if N_{HI} is much lower than 10^{21} cm^{-2} , then the scattering optical depths for both He II λ 972 and Ne VII λ 973 become so small, which would reduce Raman conversion efficiency significantly.

The same Monte Carlo code introduced by Lee (2012) is used in the current work, where the scattering region is assumed to be a uniform sphere with the point-like far UV emission source located at the center. The neutral hydrogen column density N_{HI} is measured radially from the center to the edge of the sphere. The code is designed to take full considerations of Rayleigh and Raman scattering channels faithful to the atomic physics. A given far UV photon generated in the emission region is treated to escape from the region immediately after its first Raman scattering or reaching the spherical edge after a series of multiple Rayleigh scatterings.

Fig. 6 shows our Monte Carlo simulated profiles superposed to the 2005 BOES data for two values of N_{HI} . In the case of $N_{HI} = 3.0 \times 10^{21} \text{ cm}^{-2}$, the Raman scattered He II feature sits near the edge of the plateau region, yielding a poor fit to the observed data. In view of this result and for want of a better constraint, we adopt $N_{HI} = 1.21 \times 10^{21} \text{ cm}^{-2}$, as was proposed by Jung & Lee (2004), in order to investigate the basic properties of Raman scattering of Ne VII λ 973.

In Fig. 7 we show our Monte Carlo result that appears to give the best fit to the 2003 BOES data. In the lower panel, only the Monte Carlo simulated profile is shown by a dotted line. In the upper panel, the simulated profile is superposed on the 2003 spectrum. We find the overall agreement of the Monte Carlo profile and the BOES spectrum, although the observed Raman scattered Ne VII λ 973 is of poor quality. The best fitting Gaussian width for the inci-

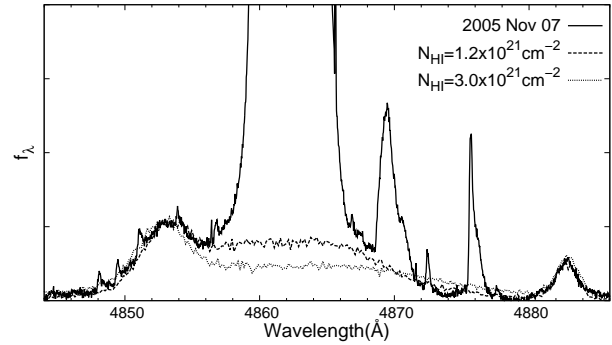


Figure 6. Monte Carlo simulations of Raman scattering of far UV continuum around Ly β with the two emission components of He II λ 972 and Ne VII λ 973. The thick dashed line shows the result for $N_{HI} = 1.2 \times 10^{21} \text{ cm}^{-2}$ and the thin dashed line is for $N_{HI} = 3.0 \times 10^{21} \text{ cm}^{-2}$. In the latter case, the Raman scattered He II feature is blended to the plateau region of Raman scattered far UV continuum, providing a poor fit to the observed data.

dent He II λ 972 is $\Delta\lambda = 0.10 \text{ \AA}$. Defining the random velocity scale for He II by

$$v_{ran} \equiv \frac{\Delta\lambda}{\lambda_0} c, \quad (6)$$

we find $v_{ran}^{HeII} = 31 \text{ km s}^{-1}$. Correspondingly for Ne VII λ 973 we have $\Delta\lambda = 0.046 \text{ \AA}$, which yields $v_{ran}^{NeVII} = 14 \text{ km s}^{-1}$, smaller by a factor of ~ 2 than the He II counterpart. The equivalent widths of He II λ 972 and Ne VII λ 973 are $EW_{He} = 0.80 \text{ \AA}$ and $EW_{Ne} = 2.6 \text{ \AA}$, respectively. However, the equivalent widths are uncertain by a factor of 2, considering the poor quality of the 2003 spectrum around the Raman features.

Similar Monte Carlo simulations with a modification of the two emission components in the input spectrum are performed to fit the 2005 BOES data. Fig. 8 shows our Monte Carlo result for the best fit, from which we find that both the He II and Ne VII regions recede from the H I region with a velocity $v = 20 \text{ km s}^{-1}$. The equivalent width of He II λ 972 for this case is 0.5 \AA . Correspondingly for Ne VII it is 1.4 \AA , which means that Ne VII λ 973 is almost 3 times stronger than He II λ 972. However, the poor quality of the 2003 spectrum prevents us from drawing any conclusion about the temporal change in the total line fluxes of He II λ 972 and Ne VII λ 973 in the two year period. We summarize the best fitting parameters in Table 3.

No significant change in the line widths of the Raman features are found in the two spectra. We simply assume that the random velocity scale v_{ran} is contributed by a thermal component v_{th} and a turbulent component v_{turb} so that we may write

$$v_{ran}^2 = v_{th}^2 + v_{turb}^2. \quad (7)$$

We further assume that the temperature and v_{turb} are the same for both He II and Ne VII regions, then the thermal velocity scale v_{th}^{He} of He II will be larger than that v_{th}^{Ne} of Ne VII by a factor $\sqrt{5}$. Using the fitted result we find $v_{turb} = 7 \text{ km s}^{-1}$, $v_{th}^{Ne} = 12 \text{ km s}^{-1}$, and $v_{th}^{He} = 27 \text{ km s}^{-1}$, from which we find the temperature of the emission region $T = 3.0 \times 10^4 \text{ K}$.

Table 3. Best Fitting Parameters from Monte Carlo Simulations

2003 Spectrum	He II 972	Ne VII 973
$\Delta\lambda$	0.10 Å	0.046 Å
Equivalent Width	0.8 Å	2.6 Å
2005 Spectrum	He II 972	Ne VII 973
$\Delta\lambda$	0.10 Å	0.046 Å
Equivalent Width	0.5 Å	1.4 Å

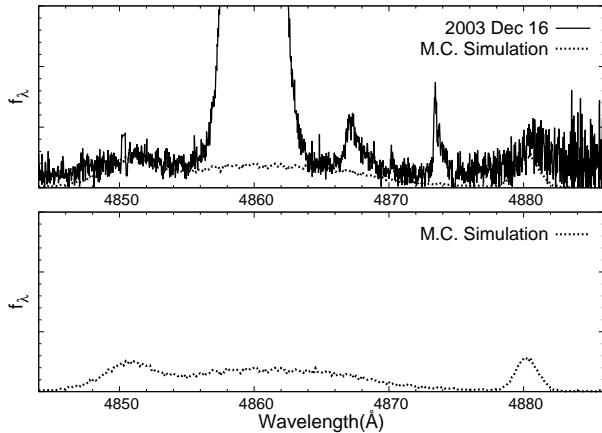


Figure 7. Monte Carlo simulated fit of Raman scattered He II λ 972 and Ne VII λ 973. The adopted neutral hydrogen column density is $N_{HI} = 1.2 \times 10^{21} \text{ cm}^{-2}$. In the upper panel, we show the 2003 data by a solid line and the Monte Carlo result by a dotted line. In the lower panel, the BOES data is deleted in order to show clearly the Monte Carlo result. For the 2003 data, both the He II and Ne VII emission regions are assumed to coincide and be at rest with respect to the H I region.

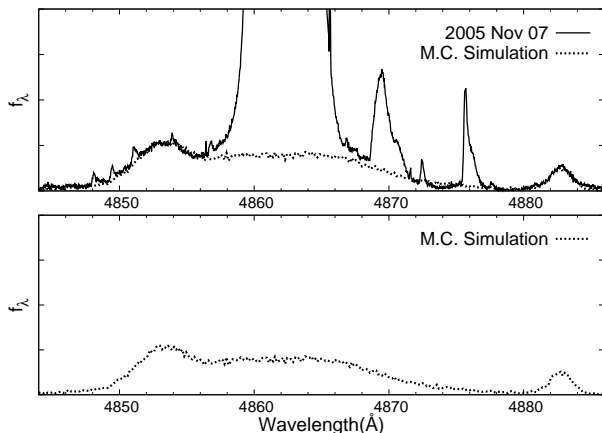


Figure 8. Monte Carlo simulated fit to the 2005 BOES data. The symbols are the same as Fig.7. In this simulation, both the He II and Ne VII emission regions are assumed to coincide but recede from the H I region with a velocity $v = +20 \text{ km s}^{-1}$.

4 SUMMARY

The operation of Raman scattering by atomic hydrogen is a very unique astrophysical process that distinguishes symbiotic stars from other celestial bodies. Thus far the Raman scattered line features found in symbiotic stars are limited to only He II and O VI. In this work we propose that the broad feature around 4881 Å in the spectrum of V1016 Cyg is formed through Raman scattering of Ne VII λ 973. We have provided the atomic physical quantities regarding Raman scattering of Ne VII λ 973. By performing Monte Carlo simulations, we obtain the random velocity scale of Ne VII and infer the equivalent width of the emission line Ne VII λ 973.

Assuming that both Ne VII λ 973 and He II λ 972 emission regions coincide, we find that both He II and Ne VII emission components are receding from the neutral region with the same speed $v \sim 20 \text{ km s}^{-1}$ in the 2005 BOES data. However, the 2003 BOES data indicate that both Ne VII and He II emission regions are consistent with their being at rest with respect to the H I region at that time.

ACKNOWLEDGEMENTS

We are grateful to an anonymous referee for very useful comments that improved the presentation of the paper. We also thank the staff of the Bohyunsan Optical Observatory for their help in securing the high resolution spectra of V1016 Cyg. This research was supported by the Basic Science Research Program through the National Research Foundation (NRF) funded by the Ministry of Education, Science and Technology (2011-0027069).

REFERENCES

- Angeloni, R., Contini, M., Ciroi, S., Rafanelli, P., MNRAS, 402, 2075
- Belczyński, K., Mikoajewska, J., Munari, U., Ivison, R. J., Friedjung, M., 2000, A&AS, 146, 407
- Bethe, H. A. & Salpeter, E. E., 1957, Quantum Mechanics of One- and Two-Electron Atoms, New York, Academic Press
- Birriel J., 2004, ApJ, 612, 1136
- Edlén, B., 1983, Physica Scripta, 28, 51
- Feldman U., Behring W. E., Curdt W., Schüle U., Wilhelm K., Lemaire P. & Moran K. T. M., 1997, ApJ, 113, 195
- Harries, T. J. & Howarth, I. D., 1997, A&AS, 121, 15
- Herald J. E., Bianchi L. & Hillier D. J., 2005, ApJ, 627, 424
- Iben, I., Jr., Tutukov, A. V., ApJS, 105, 145
- Jung Y.-C. & Lee H.-W., 2004, MNRAS, 355, 221
- Kaastra, J. S., Roos, N., & Mewe, R. 1995, A&A, 300, 25,
- Kenyon, S. J., 1986, The Symbiotic Stars, Cambridge University Press
- Kramida, A. & Buchet-Poulizac, M.-C., 2006, European Physical Journal D, 38, 265
- Kramida, A., Ralchenko, Yu., Reader, J., and NIST ASD Team, 2013, *NIST Atomic Spectra Database (ver. 5.1)*
- Lee H.-W., 2000, ApJ, 541, L25
- Lee H.-W., 2012, ApJ, 750, 127
- Lee H.-W., Jung Y.-C., Song I.-O. & Ahn S., 2006, ApJ, 636, 1045

- Lee H.-W. & Kang S., 2007, *ApJ*, 669, 1156
Lee H.-W. & Park M.-G., 1999, *ApJ*, 515, L89
Luna, G. J. M., Sokoloski, K., Mukai, K. & Nelson, T.,
2013, *A&A*, 559, A6
Mastrodemos, N., Morris, M., 1998, *ApJ*, 497, 303
Mikolajewska, M., *Baltic Astronomy*, 21, 5
McCusky, S., 1965, *IAU Circ.* 1916
Mürset, U. Nussbaumer, H., Schmid, H. M. & Vogel, M.,
1991, *A&A*, 248, 458
Nussbaumer, H., 2003, *ASPC*, 303, 557
Schmid, H. M., 1989, *A&A*, 211, L31
Schmid, H. M., 1992, *A&A*, 254, 224
Skopal, A., 2006, *A&A*, 457, 1003
Sokoloski, J. L., Bildsten, L., & Ho, W. C. G., 2001, *MNRAS*, 326, 553
Torres A. F., Kraus M., Cidale L. S., Barbá R., Borges
Fernandes M. & Brandi E., 2012, *MNRAS*, 427, L80
van Groningen, E., 1993, *MNRAS*, 264, 975
Warner, B., 1995, *Cataclysmic Variable Stars*, Cambridge
University Press,
Werner, K., Rauch, T., Reiff, E., Kruk, J. W. & Napi-
wotzki, R., 2004, *A&A*, 427, 685
Young, P. R., Dupree A. K., Espey B. R., Kenyon, S. J.,
Ake, T. B., 2005, *AJ*, 618, 891

This paper has been typeset from a \TeX / \LaTeX file prepared
by the author.